Neuro-Oncology
27(1), 89–105, 2025 | https://doi.org/10.1093/neuonc/noae214 | Advance Access date 19 November 2024

Longitudinal multimodal profiling of IDH-wildtype glioblastoma reveals the molecular evolution and cellular phenotypes underlying prognostically different treatment responses

Calixto-Hope G. Lucas[†], Nadeem N. Al-Adli[†], Jacob S. Young[†], Rohit Gupta[†], Ramin A. Morshed, Jasper Wu, Ajay Ravindranathan, Anny Shai, Nancy Ann Oberheim Bush, Jennie W. Taylor, John de Groot, Javier E. Villanueva-Meyer, Melike Pekmezci, Arie Perry, Andrew W. Bollen, Philip V. Theodosopoulos, Manish K. Aghi, Edward F. Chang, Shawn L. Hervey-Jumper, David R. Raleigh, Annette M. Molinaro, Joseph F. Costello, Aaron A. Diaz, Jennifer L. Clarke, Nicholas A. Butowski, Joanna J. Phillips, Susan M. Chang, Mitchel S. Berger, and David A. Solomon

All author affiliations are listed at the end of the article

Corresponding Authors: Susan M. Chang, MD, Division of Neuro-Oncology, Department of Neurological Surgery, University of California, San Francisco, 400 Parnassus Avenue, ACC 800, San Francisco, CA 94143, USA (susan.chang@ucsf.edu); Mitchel S. Berger, MD, Department of Neurological Surgery, University of California, San Francisco, 505 Parnassus Avenue, Moffitt 777, San Francisco, CA 94143, USA (mitchel.berger@ucsf.edu); David A. Solomon, MD, PhD, Department of Pathology, University of California, San Francisco, 513 Parnassus Avenue, HSW 451, San Francisco, CA 94143, USA (david.solomon@ucsf.edu).

[†]These authors contributed equally to this work.

Abstract

Background. Despite recent advances in the biology of IDH-wildtype glioblastoma, it remains a devastating disease with median survival of less than 2 years. However, the molecular underpinnings of the heterogeneous response to the current standard-of-care treatment regimen consisting of maximal safe resection, adjuvant radiation, and chemotherapy with temozolomide remain unknown.

Methods. Comprehensive histopathologic, genomic, and epigenomic evaluation of paired initial and recurrent glioblastoma specimens from 106 patients was performed to investigate the molecular evolution and cellular phenotypes underlying differential treatment responses.

Results. While *TERT* promoter mutation and *CDKN2A* homozygous deletion were early events during gliomagenesis shared by initial and recurrent tumors, most other recurrent genetic alterations (eg, *EGFR*, *PTEN*, and *NF1*) were commonly private to initial or recurrent tumors indicating acquisition later during clonal evolution. Furthermore, glioblastomas exhibited heterogeneous epigenomic evolution with subsets becoming more globally hypermethylated, hypomethylated, or remaining stable. Glioblastoma that underwent sarcomatous transformation had shorter interval to recurrence and were significantly enriched in *NF1*, *TP53*, and *RB1* alterations and the mesenchymal epigenetic class. Patients who developed somatic hypermutation following temozolomide treatment had significantly longer interval to disease recurrence and prolonged overall survival, and increased methylation at 4 specific CpG sites in the promoter region of *MGMT* was significantly associated with this development of hypermutation. Finally, an epigenomic evolution signature incorporating change in DNA methylation levels across 347 critical CpG sites was developed that significantly correlated with clinical outcomes.

Conclusions. Glioblastoma undergoes heterogeneous genetic, epigenetic, and cellular evolution that underlies prognostically different treatment responses.

© The Author(s) 2024. Published by Oxford University Press on behalf of the Society for Neuro-Oncology.
This is an Open Access article distributed under the terms of the Creative Commons Attribution-NonCommercial License (https://creativecommons.org/licenses/by-nc/4.0/), which permits non-commercial re-use, distribution, and reproduction in any medium, provided the original work is properly cited. For commercial re-use, please contact reprints@oup.com for reprints and translation rights for reprints. All other permissions can be obtained through our RightsLink service via the Permissions link on the article page on our site—for further information please contact journals.permissions@oup.com.

Key Points

- The genomic, epigenomic, and cellular landscape of glioblastoma evolves heterogeneously in response to the current standard-of-care treatment regimen.
- Molecular profiles at the time of initial surgery are predictive of differential treatment response and biologic trajectory.
- Specific epigenetic signatures correlate with the development of sarcomatous transformation, somatic hypermutation, and clinical outcomes.

Importance of the Study

Our analyses demonstrate that most glioblastomas undergo longitudinal genomic and/or epigenomic evolution associated with differential clinical outcomes. As such, precision medicine treatment regimens for glioblastoma should be based on molecular studies performed on both initial and recurrent surgical specimens, given the predictive value of certain molecular signatures at initial resection and how the molecular and cellular landscape evolves at recurrence.

Glioblastoma, IDH-wildtype (GBM) remains a molecularly heterogeneous disease refractory to current therapies. Current standard of care for glioblastoma includes maximal safe resection, adjuvant radiation, and chemotherapy with the alkylating agent temozolomide.[1] Unfortunately, despite this aggressive therapeutic approach, glioblastoma inevitably recurs and has proven to be largely resistant to most targeted and immune-based therapies that have been experimentally tested to date.[2]

Longitudinal molecular profiling studies have revealed that glioblastoma displays a high degree of clonal stability during therapy, although private mutations between primary and recurrent tumor samples are common.[3–13] Global analyses with bulk DNA sequencing techniques have demonstrated a lack of selection pressure or evolutionary bottleneck from standard treatments, highlighting the importance of transcriptional and epigenetic programs in glioblastoma resistance and progression.[14–17] Single-cell gene expression analyses have shown multiple cell states within most glioblastomas, which are thought to be highly plastic and epigenetically controlled, and an increase in the mesenchymal (MES) cell state has been observed at disease recurrence.[14,18,19] Moreover, the tumor microenvironment and immune cell changes over time may likely be another key driver of therapeutic response in glioblastoma.[20,21]

DNA methylation profiling has emerged as a means of characterizing the distinct subclasses of glioblastoma and their cellular composition,[22–27] and epigenomic signatures have recently been used to independently predict glioblastoma patient survival.[28,29] A recent longitudinal epigenomic analysis of adult-type diffuse gliomas described a largely stable epigenome over time for IDH-wildtype glioblastomas, whereas IDH-mutant astrocytomas demonstrated a more dynamic epigenome with a global decrease in methylation following standard treatment.[17] However, how the epigenome changes on an individual patient basis and in response to specific treatments for IDH-wildtype glioblastoma remains unresolved.

To investigate how longitudinal molecular evolution of glioblastoma drives tumor progression and treatment resistance, we performed comprehensive histopathologic assessment, targeted genomic sequencing, and genome-wide DNA methylation profiling of paired initial and recurrent IDH-wildtype glioblastoma tumor specimens from 106 patients as part of a sponsored Glioblastoma Precision Medicine Program at our institution. We identified the molecular evolution and cellular phenotypes underlying prognostically different subgroups of tumors, including those which undergo epigenetic class switching, those which undergo sarcomatous transformation, and those which develop somatic hypermutation in response to the alkylating effects of temozolomide. The identified molecular evolution signatures associated with prognostically different treatment responses may likely inform future precision medicine therapeutic studies for patients with glioblastoma.

Methods

Study Population and Tumor Specimens

The study cohort consisted of 106 adult patients who underwent 2 or more longitudinal surgical resections of IDH-wildtype glioblastoma at the University of California, San Francisco (UCSF) Medical Center. All patients had tumors pathologically confirmed as "Glioblastoma, IDH-wildtype" according to the 2021 WHO Classification of Central Nervous System Tumors. In total, 232 tumor specimens were examined by histopathology and genomic profiling, of which 226 were also studied by DNA methylation array profiling. This included 101 patients with histopathology, and genomic profiling performed on both an initial treatment-naïve resection specimen and a first surgically treated recurrent tumor specimen, of which 98 of these patients also had DNA methylation array profiling performed on both specimens. This study was approved by

the UCSF institutional review board. See Supplementary Methods for further details.

Tumor Volume Measurement and Extent of Resection Quantitation

Tumor volumes were manually delineated using BrainLab Smartbrush software. The extent of resection was classified as supramaximal, maximal, or submaximal based on established RANO categories for glioblastoma.[30,31] See Supplementary Methods for further details.

Histology and Immunohistochemistry

Sarcomatous transformation to gliosarcoma at recurrence was defined by fascicular tumor cell growth, intercellular reticulin deposition, and immunohistochemical evidence of glial to MES transdifferentiation. See Supplementary Methods for further details.

Targeted Next-Generation DNA Sequencing

Capture-based next-generation DNA sequencing was performed on 232 longitudinal glioblastoma tumor specimens using the UCSF500 NGS panel as previously described.[32–36] For a subset of patients, sequencing was also performed on a constitutional DNA sample from a buccal swab or peripheral blood specimen. Temozolomide-induced hypermutation was defined as those recurrent glioblastomas demonstrating somatic hypermutation (TMB values of ≥15 somatic mutations per Mb) acquired at recurrence following temozolomide chemotherapy that was not present in the matched initial treatment-naïve tumor with characteristic mutational signature.[3,37–39] See Supplementary Methods for further details.

Genomic Alteration Evolution

The likely oncogenic/pathogenic genetic alterations identified in the initial treatment-naïve tumor were compared to those in the first surgically treated recurrence. Those patients with an identical set of alterations were classified as "stable". Those patients with newly acquired alterations in the recurrent tumor but otherwise maintained all alterations present in the initial tumor were classified as "additive". Those patients with alterations private to the initial tumor were classified as "divergent". See Supplementary Methods for further details.

Genome-Wide DNA Methylation Profiling

Genomic DNA from 226 longitudinal IDH-wildtype glioblastoma tumor specimens was bisulfite converted and hybridized to Infinium MethylationEPIC 850k version 1.0 Beadchips (Illumina). Genomic DNA from 31 longitudinal IDH-mutant astrocytoma tumor specimens from 24 patients, consisting of 14 initial treatment-naïve specimens and 17 recurrent posttreatment specimens, was identically bisulfite converted and hybridized to MethylationEPIC arrays for comparison. See Supplementary Methods for further details.

DNA Methylation Class Evolution

Random forest classification of DNA methylation profiles was performed using the DKFZ MolecularNeuropathology.org online classifier version 12.5.[24,40] When both the initial tumor and first recurrence were assigned to the same glioma methylation class with a calibrated score >0.3, then that patient's tumor pair was defined as "stable". When the first recurrence was assigned to a different glioma methylation class with calibrated score >0.3 than the initial tumor, then that patient's tumor pair was defined as "switch". See Supplementary Methods for further details.

DNA Methylation Data Analysis

Differential methylation analysis between initial and recurrent tumor specimens and also among defined subgroups was performed using dmpFinder (minfi v.1.40.0). See Supplementary Methods for further details.

MGMT Promoter Methylation-Based Risk Groups for Developing Temozolomide-Induced Hypermutation

Risk group assessment was performed based on DNA methylation levels at the 4 significantly differentially methylated CpG sites in the *MGMT* promoter region between initial treatment-naïve tumors which subsequently developed hypermutation at recurrence posttemozolomide ($n = 12$) and those that did not ($n = 87$). See Supplementary Methods for further details.

Global Mean DNA Methylation Evolution

The global mean DNA methylation level was calculated for each individual tumor specimen by averaging the β-values across all the ~850,000 interrogated CpG sites. A change in mean global DNA methylation β-value from initial to recurrent tumor of >0.02 was defined as "hypermethylation shift," <–0.02 as "hypomethylation shift," and between 0.02 and –0.02 as "stable". See Supplementary Methods for further details.

Glioblastoma Outcome-Associated DNA Methylation Evolution Signature Development

Three hundred forty-seven CpG sites whose change in DNA methylation β-value (Δβ value) from initial to first recurrence tumor specimens most strongly correlated with overall survival were identified. Based on the mean Δβ value across the 347 CpG sites for each tumor pair, we defined 3 patient subgroups using the following cutoffs: Group A, mean $\Delta\beta > 0.0305$ (become more methylated at the 347 CpG sites at recurrence); Group B, $-0.0145 <$ mean $\Delta\beta \leq 0.0305$ (relatively stable methylation levels); and

Group C, mean $\Delta\beta \leq -0.0145$ (become less methylated). See Supplementary Methods for further details.

Statistics

All statistical analyses were performed using R software (version 4.4.0). See Supplementary Methods for further details.

Results

Longitudinal IDH-Wildtype Glioblastoma Patient Cohort

A cohort of 106 patients with pathologically confirmed IDH-wildtype glioblastoma who underwent 2 or more longitudinal surgical resections was assembled for analysis (Figure 1A, Supplementary Tables S1–S3). The patients had a median age at initial diagnosis of 54.1 years and included 43 females (41%) and 63 males (59%). The tumors were uniformly supratentorial, with 104 centered in the cerebral hemispheres and 2 in the thalamus. All patients underwent maximal safe resection (17% supramaximal, 60% maximal, and 23% submaximal), 99% received adjuvant external beam radiation, and 89% received adjuvant temozolomide. The median interval to first surgically treated recurrence was 10.9 months. After repeat surgical resection, 22% of patients received additional radiation therapy and 99% received additional chemotherapy, which variably consisted of additional temozolomide, lomustine (CCNU), and different experimental agents. All but one patient (#13, alive at last clinical follow-up) died of disease during the study period. The median interval from first surgically treated recurrence to death was 10.4 months, and the median overall survival from initial surgery was 21.6 months.

Genetic Alterations across Matched Initial and Recurrent Pairs of IDH-Wildtype Glioblastoma

Genomic profiling of 101 matched initial and recurrent IDH-wildtype glioblastoma pairs demonstrated a similar frequency of large-scale copy number alterations when comparing the initial versus recurrent tumor specimens (Figure 1B, Supplementary Figure S1 and Table S4). This included gain of chromosomes 7, 19, and 20, as well as loss of chromosomes 6q, 9p, 10, and 13q. No copy number alterations were uniquely enriched in the initial tumor specimens, whereas only gain of chromosome 5 was uniquely enriched in the recurrent tumor specimens. Mutational analysis also revealed a similar frequency of the most common genetic alterations when comparing the initial versus recurrent tumor specimens (Figure 1C, Supplementary Figure S2 and Tables S5–S8). The most commonly altered oncogenes and tumor suppressor genes included *TERT*, *CDKN2A*, *EGFR*, *PTEN*, *TP53*, *NF1*, *PIK3CA*, *RB1*, and *PTPN11*; none of which had significantly different frequencies between the initial and recurrent tumor cohorts. When comparing the distribution of genetic alterations across each individual matched initial and recurrent pair, *TERT* promoter mutation and *CDKN2A/B* homozygous deletions were nearly uniformly shared between the initial and recurrent tumor specimens for each of the altered pairs (Figure 1D, Supplementary Table S8). In contrast, while the other oncogene and tumor suppressor gene alterations were shared in some tumor pairs, a substantial subset of the tumor pairs demonstrated oncogenic driver events that were private to either the initial or recurrent tumor specimens. Most frequently, this included *EGFR*, *PTEN*, *TP53*, *NF1*, *PIK3CA*, *RB1*, and *PTPN11* alterations. These findings indicate that *TERT* promoter mutation and *CDKN2A/B* homozygous deletion are early tumor-initiating events in most IDH-wildtype glioblastomas, whereas genetic events affecting most of the other major oncogenes and tumor suppressor genes often occur later during gliomagenesis.

Epigenomic Class Switching across Matched Initial and Recurrent Pairs of IDH-Wildtype Glioblastoma

Of the 98 paired initial treatment-naïve and first surgically treated recurrent tumors that underwent DNA methylation profiling, 79 demonstrated matches to glioma classes for both the initial and recurrent tumor using the DKFZ Molecular Neuropathology classifier v12.5 (Figure 1E, Supplementary Table S9). The initial cohort demonstrated an enrichment for the RTK2 methylation class (initial cohort: 51% RTK2, 32% MES, 15% RTK1, 3% pediHGG), whereas the recurrent cohort demonstrated an enrichment for the MES methylation class (recurrent cohort: 42% RTK2, 46% MES, 11% RTK1, 0% pediHGG). A subset of patients had stable methylation class between initial and recurrent tumors ($n = 38$) compared with the remaining patients who had methylation class switching from initial to recurrent tumor specimens ($n = 41$). When segregating the patient cohort by DNA methylation class as "stable" versus "switch," there were no significant differences in overall survival or recurrence-free survival from initial surgery, or survival from first surgically treated recurrence (Figure 1F, Supplementary Figure S3).

Genomic Evolution across Matched Initial and Recurrent Pairs of IDH-Wildtype Glioblastoma

Three distinct patterns of genomic evolution were identified when comparing the genetic alteration results for the paired initial and recurrent glioblastoma specimens (Figure 2A). A minority of patients ($n = 16$) demonstrated an identical set of oncogenic driver alterations between their initial and recurrent tumor specimens, which we termed "stable". Another subset ($n = 19$) demonstrated an identical set of oncogenic driver alterations between their initial and recurrent tumor specimens except for newly acquired genetic alterations private to the recurrent tumor specimens, such as newly acquired *TP53* mutation at recurrence in patient #44. We termed this pattern of genomic evolution as "additive". Finally, the majority of patients ($n = 66$) demonstrated "divergent" evolution between initial and recurrent tumor specimens, with some commonly shared driver events but also with oncogenic alterations that were

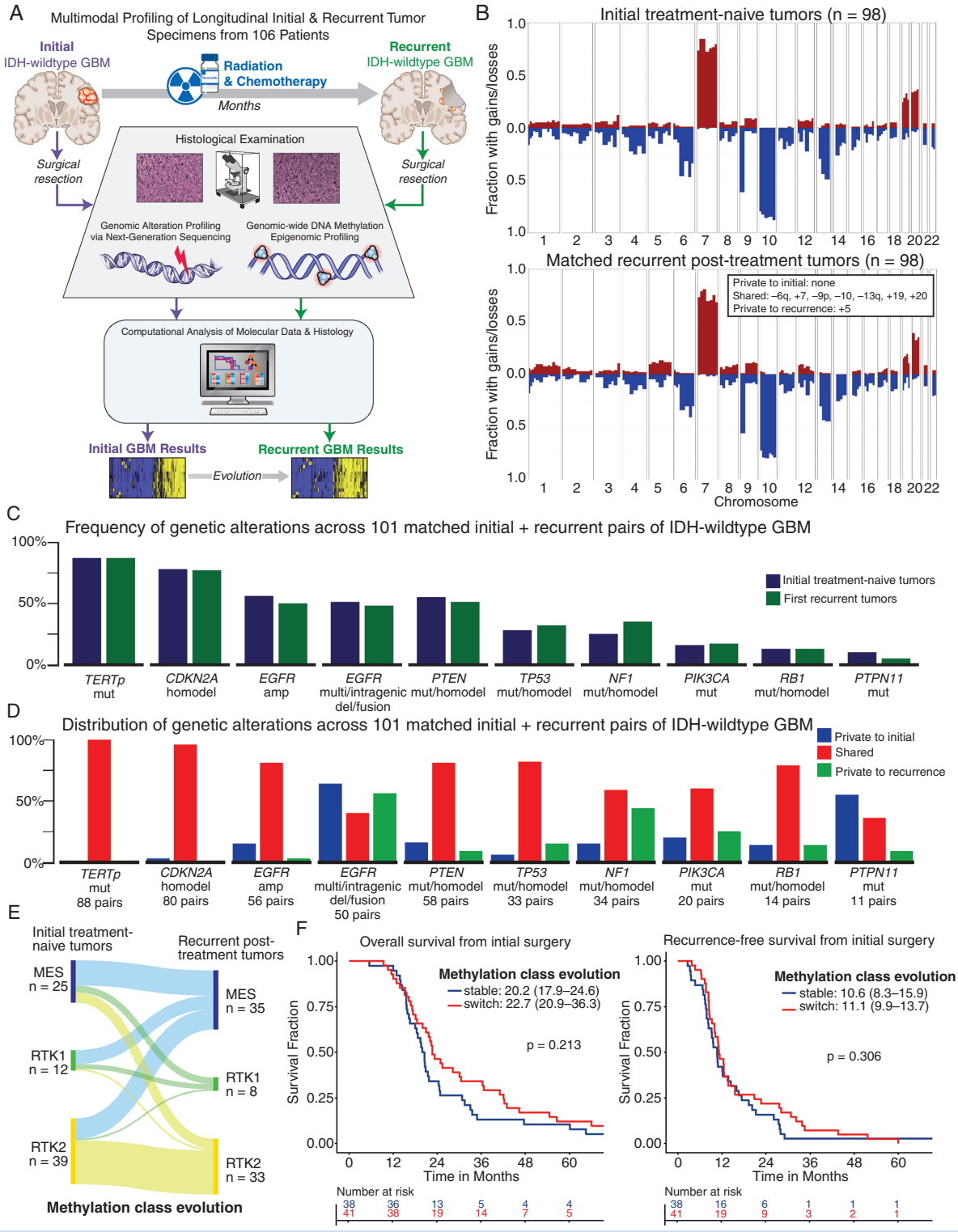


Figure 1. Longitudinal molecular profiling of paired initial and recurrent IDH-wildtype glioblastoma specimens from 106 patients reveals the fundamental genomic alterations underlying glioblastoma pathogenesis. (A) Schematic of the overall study design consisting of comprehensive histopathologic, genomic, and epigenomic profiling of two or more longitudinal IDH-wildtype glioblastoma tumor specimens from 106 patients. (B) Summary copy number variation plots of matched initial treatment-naïve (top) and first surgically treated recurrent (bottom) IDH-wildtype glioblastomas from 98 patients. (C) Bar plot of genetic alteration frequency for the 9 most commonly altered oncogenes and tumor suppressor genes in 101 pairs of matched initial treatment-naïve and first surgically treated recurrent IDH-wildtype glioblastomas. Abbreviations: amp = amplification; homodel = homozygous/biallelic deletion; intragenic del = intragenic deletion (eg *EGFRvIII* exons 2-7 deletion); mut = mutation. (D) Bar plot showing the distribution of genetic alterations in these 9 most commonly altered oncogenes and tumor suppressor genes segregated by private to initial, private to recurrence, or shared between initial and recurrent tumor specimens in the 101 IDH-wildtype glioblastoma longitudinal pairs.

(E) Sankey plot of DNA methylation class assignment for 76 pairs of matched initial treatment-naïve and first surgically treated recurrent IDH-wildtype glioblastomas using the DKFZ Molecular Neuropathology classifier tool version 12.5 using a calibrated score cutoff of 0.3 for inclusion. This analysis revealed frequent epigenetic class switching at recurrence, with a predominance of the Receptor Tyrosine Kinase 2 (RTK2) methylation class at initial surgery and a predominance of the MES methylation class at recurrence. (F) Kaplan–Meier plots of overall survival from initial surgery (left) and recurrence-free survival from initial surgery (right) for 79 patients with IDH-wildtype glioblastoma stratified by methylation class evolution from initial to recurrent tumor pairs as either "stable" or "switch" based on assignment by the DKFZ Molecular Neuropathology classifier tool. Median estimated survival and 95% confidence intervals (CIs) are shown, as well as exact *P*-values by log-rank test.

private to both the initial and recurrent tumor specimens. Examples include patient #35 with shared focal high-level *EGFR* amplification in both tumor specimens, but the initial tumor contained intragenic deletion of exons 2-7 (*EGFRvIII* variant) on the amplified *EGFR* alleles that was not present in the recurrent tumor, and the recurrent tumor contained a p.V292M extracellular domain missense mutation on the amplified *EGFR* alleles that was not present in the initial tumor. Patient #66 had focal high-level *EGFR* amplification in both tumor specimens which each contained the *EGFRvIII* variant; however, there were different intragenic deletion breakpoints flanking exons 2 and 7 for the initial and recurrent tumor specimens, indicating that these were independently acquired genetic events during the evolution of this patient's glioblastoma. Patient #14 had shared *TERT* promoter mutation and *CDKN2A* homozygous deletion between initial and recurrent tumor specimens, with additional *EGFR* high-level amplification that was private to the initial tumor and *MET* high-level amplification and *PTEN* mutation that were newly acquired in the recurrent tumor. Patient #98 had shared *TERT* promoter mutation, *CDKN2A* homozygous deletion, and *LZTR1* frameshift mutation between initial and recurrent tumor specimens, with additional *NF1* and *PTEN* mutations in both tumor specimens; however, the *NF1* nonsense mutation and *PTEN* missense mutation in the initial tumor were divergent from the inactivating *NF1* and *PTEN* mutations present in the recurrent tumor. When segregating the patient cohort by these 3 distinct genomic evolution patterns (stable, additive, and divergent), no difference was found in overall or recurrence-free survival from initial surgery, or survival from first surgically treated recurrence (Figure 2B).

Distinct Epigenomic Evolution of IDH-Wildtype Glioblastoma Compared to IDH-Mutant Astrocytoma

DNA methylation array data interrogating ~850,000 CpG sites across the genome were simultaneously generated from 98 initial treatment-naïve and matched recurrent posttreatment IDH-wildtype glioblastomas alongside 14 initial treatment-naïve IDH-mutant astrocytomas and 17 recurrent IDH-mutant astrocytomas to directly compare the epigenomic evolution of these 2 distinct glioma tumor types. We found that initial IDH-mutant astrocytomas had markedly hypermethylated epigenomes with substantially more methylated CpG sites across the genome compared to IDH-wildtype glioblastomas (Figure 3A, Supplementary Figure S4A). Recurrent IDH-mutant astrocytomas had reduced methylation levels similar to the global methylation levels of IDH-wildtype glioblastomas. In contrast, the mean DNA methylation levels did not appreciably change between initial and recurrent IDH-wildtype glioblastoma specimens for the vast majority of the ~850,000 interrogated CpG sites. We next compared the mean global methylation evolution of each individual tumor pair, which revealed that IDH-mutant astrocytomas uniformly became less globally methylated from initial to recurrent tumor specimens, i.e. "hypomethylation shift" (Figure 3B). In contrast, we found that IDH-wildtype glioblastomas underwent heterogenous epigenomic evolution, with subsets becoming more globally methylated (27%, ie "hypermethylation shift"), less globally methylated (22%, ie "hypomethylation shift"), or remaining stable (51%) (Supplementary Table S10). Among ~850,000 interrogated CpG sites, we identified only 110 and 151 sites that consistently became more methylated or less methylated between initial and recurrent IDH-wildtype glioblastomas (Figure 3C, D, Supplementary Tables S11 and S12), which regulate genes involved in neuronal morphogenesis, oligodendrocyte differentiation, and myelination (Figure 3E, Supplementary Tables S13–S15, Figure S5). In comparison, we identified 260 and 18,527 CpG sites that consistently became more methylated or less methylated between initial and recurrent IDH-mutant astrocytomas (Figure 3C, D, Supplementary Tables S16 and S17), which regulate genes involved in neuronal stem-like differentiation, cell cycle control, and other biologic processes (Supplementary Figures S4B and S5 and Tables S18–S20). The CpG sites that consistently became more or less methylated between initial and recurrent IDH-wildtype glioblastomas and IDH-mutant astrocytomas demonstrated minimal overlap (Figure 3C) and had unique distribution patterns across the genome (Figure 3D), indicating that this was unlikely to represent random or stochastic epigenomic evolution. We identified *RBFOX3*, which encodes an RNA binding domain commonly known as NeuN, as a target of epigenomic evolution specifically in IDH-mutant astrocytomas, with 12 CpG sites in the upstream regulatory sequence that became significantly less methylated from initial to recurrent IDH-mutant astrocytomas but did not change in methylation levels between initial and recurrent IDH-wildtype glioblastomas (Supplementary Figure S4C). Notably, a recent study found that mean global DNA methylation levels in initial treatment-naïve IDH-wildtype glioblastomas correlated with patient outcomes, with those patients having more globally hypermethylated tumor epigenomes demonstrating superior survival compared with those patients having more globally hypomethylated tumor epigenomes.[29] To evaluate the potential clinical impact of mean global methylation evolution from initial to recurrent tumor specimens, we performed Kaplan–Meier survival analysis segregating our longitudinal IDH-wildtype glioblastoma patient cohort

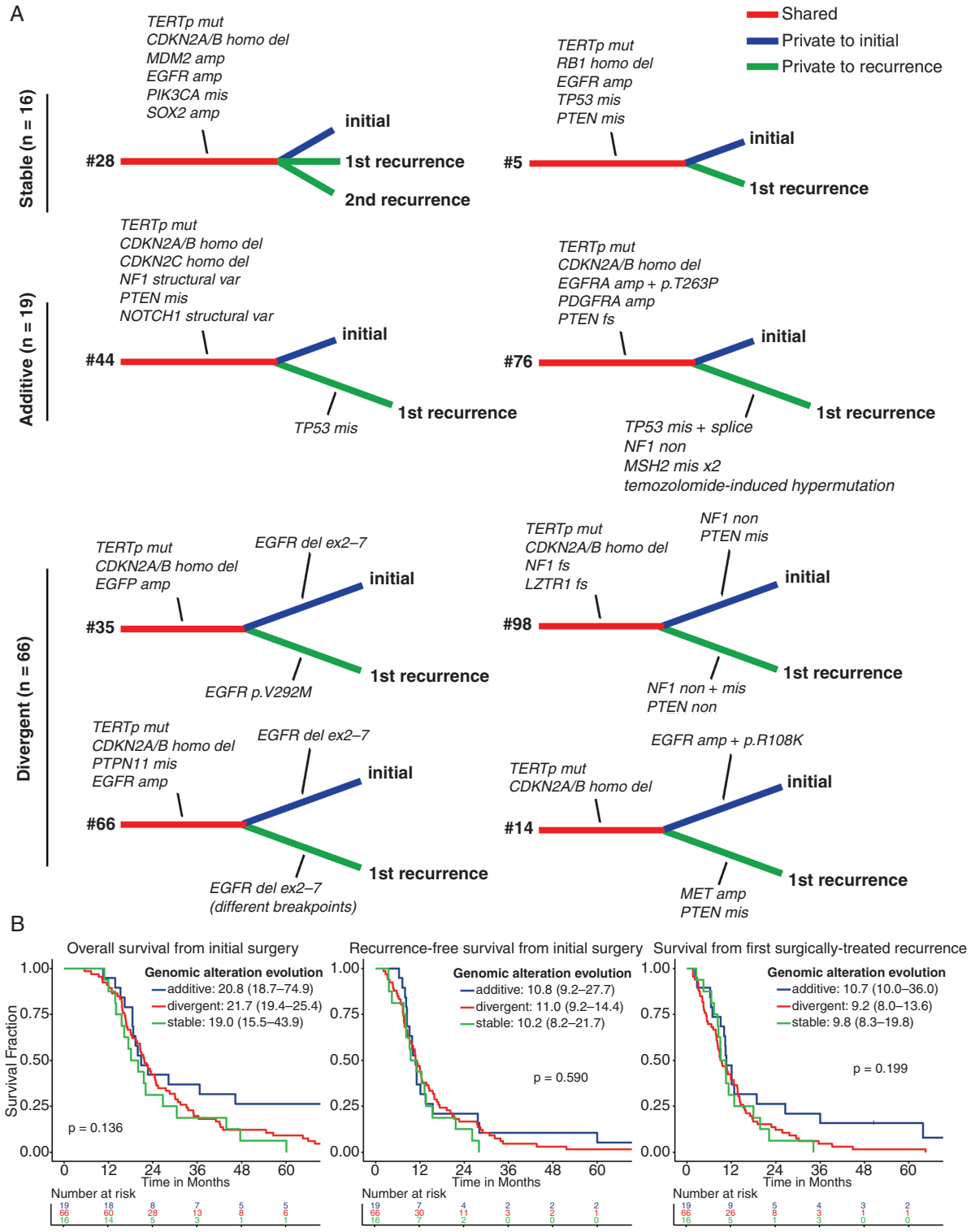


Figure 2. Longitudinal genomic profiling of paired initial and recurrent IDH-wildtype glioblastoma specimens from 106 patients reveals the interpatient heterogeneity of genomic evolution in response to treatment. (A) Genetic evolution dendrograms derived from targeted DNA sequencing analysis of paired initial and recurrent IDH-wildtype glioblastoma specimens illustrating 3 distinct patterns of genomic evolution which were termed "stable", "additive", and "divergent". Genomic alterations that occurred early during gliomagenesis and were shared between initial and recurrent tumors are shown along the truncal red axis, whereas alterations that occurred later during tumorigenesis and were private to either initial or recurrent tumors are shown along the branched blue and green axes, respectively. Abbreviations: amp = amplification; fs = frameshift mutation; homo del = homozygous/biallelic deletion; mis = missense mutation; mut = mutation; non = nonsense mutation; splice = splice site mutation; var = variant. (B) Kaplan–Meier plots of overall survival from initial surgery (left), recurrence-free survival from initial surgery (middle), and survival from first surgically treated recurrence (right) for 101 patients with IDH-wildtype glioblastoma stratified by genomic alteration evolution as either "stable," "additive," or "divergent" based on targeted DNA sequencing analysis. Median estimated survival and 95% CIs are shown, as well as exact *P*-values by log-rank test.

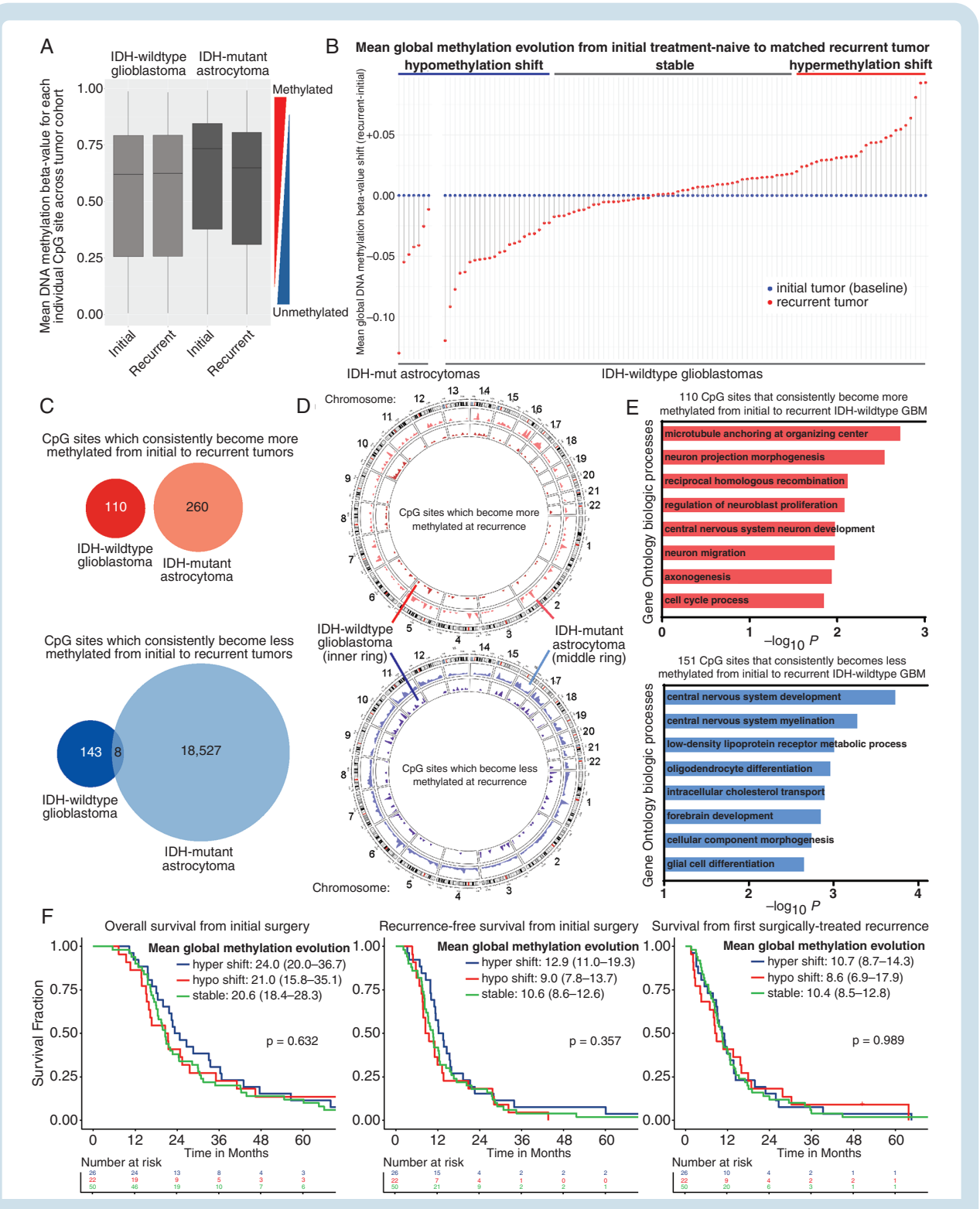


Figure 3. Distinct heterogeneous epigenomic evolution of IDH-wildtype glioblastomas versus IDH-mutant astrocytomas in response to therapy. (A) Box plot showing mean DNA methylation levels at each of ~850,000 interrogated CpG sites across the genome of 98 initial treatment-naïve IDH-wildtype glioblastomas, 98 matched recurrent posttreatment IDH-wildtype glioblastomas, 14 initial treatment-naïve IDH-mutant astrocytomas, and 17 recurrent posttreatment IDH-mutant astrocytomas. (B) Lollipop plot of the mean global DNA methylation β-value for all 850,000 CpG sites from initial tumor specimen (blue) to recurrent tumor specimen (red) for 98 patients with IDH-wildtype glioblastoma and 7 patients with IDH-mutant astrocytoma for comparison. The amount of shift on the *y*-axis between the initial and recurrent tumor specimen represents the change in mean global DNA methylation levels across the entire genome for each individual patient. Some IDH-wildtype glioblastomas became more globally methylated from initial to recurrent tumor specimens (hypermethylation shift), some are relatively stable, and some become less globally methylated (hypomethylation shift). (C) Venn diagrams showing the number and overlap of the ~850,000 interrogated CpG sites that consistently

become more methylated (red) or less methylated (blue) from initial to recurrent tumor specimens in 98 pairs of IDH-wildtype glioblastomas and 7 pairs of IDH-mutant astrocytomas (supplemented with additional unpaired tumor specimens, 7 initial and 10 recurrent). (D) Circos plots showing the genome mapping of the specific CpG sites that undergo consistent epigenomic evolution in IDH-wildtype glioblastoma versus IDH-mutant astrocytoma. Outermost rings show the chromosome position. The top plot with red peaks shows the CpG sites that become more methylated from initial to recurrent tumor specimens, while the bottom plot with blue peaks shows the CpG sites that become less methylated from initial to recurrent specimens. Middle rings show the 260 CpG sites that consistently become more methylated (light red) and 18,535 CpG sites that consistently become less methylated (light blue) in IDH-mutant astrocytomas. Innermost rings show the 110 CpG sites that consistently become more methylated (dark red) and 151 CpG sites that consistently become less methylated (dark blue) in IDH-wildtype glioblastomas. (E) Gene Ontology biological processes that are significantly enriched ($P < .05$) in genes containing the most differentially methylated CpG sites between 98 initial treatment-naive IDH-wildtype glioblastomas and their matched recurrent posttreatment tumor specimens. (F) Kaplan–Meier plots of overall survival from initial surgery (left), recurrence-free survival from initial surgery (middle), and survival from first surgically treated recurrence (right) for 98 patients with IDH-wildtype glioblastoma stratified by mean global methylation evolution as hypermethylation shift, stable, or hypomethylation shift. Median estimated survival and 95% CIs are shown, as well as exact *P*-values by log-rank test.

by mean global methylation shift (Figure 3F). However, no significant difference was noted in overall or recurrence-free survival from initial surgery, or survival from first surgically treated recurrence.

Transformation to Gliosarcoma Is Determined by a Distinct Molecular Signature at Initial Resection

Histopathologic assessment of the IDH-wildtype glioblastoma tumor cohort revealed 18 patients (17%) that developed sarcomatous transformation at recurrence (Figure 4A). Compared with conventional glioblastoma, patients who developed gliosarcoma had significantly shorter interval between initial surgery and first recurrence (9.0 vs. 11.7 months, $P = .001$; Figure 4B). While there were no differences in sex, age, tumor location, or adjuvant therapy (Supplementary Table S1), we found differences in the molecular signatures of initial treatment-naïve glioblastoma that transformed to gliosarcoma at recurrence, including a significant enrichment in *NF1*, *TP53*, and *RB1* alterations and an absence of *EGFR* amplification, with 3 tumors harboring *EGFR* mutations occurring in the absence of *EGFR* gene amplification (Figure 4C, Supplementary Table S21). Glioblastoma which underwent sarcomatous transformation were enriched for the MES epigenetic class at initial surgery compared with those conventional glioblastoma which did not transform (69% vs. 25%) (Figure 4D, Supplementary Table S9). There was also an enrichment for the novel Mesenchymal subclass B (MES B) at recurrence among the glioblastoma which underwent sarcomatous transformation compared with those that did not transform (43% vs. 2%). Among ~850,000 interrogated CpG sites, we identified 1503 and 2090 CpG sites within upstream regulatory regions that were significantly more methylated or less methylated in those initial treatment-naïve glioblastomas that transformed to gliosarcoma at recurrence compared with those conventional glioblastomas which did not transform (Figure 4E, Supplementary Tables S22 and S23). Gene Ontology biological processes enriched in these differentially methylated genes include macrophage migration, TGF-β signaling, and cell–cell adhesion (Figure 4F, Supplementary Tables S24–S26 and Figure S6). These findings indicate that IDH-wildtype glioblastoma which transform to gliosarcoma at recurrence posttreatment have a unique genetic and epigenetic composition at initial surgery.

Development of Somatic Hypermutation Following Temozolomide Treatment Is Dictated by Specific *MGMT* and *KCNQ1DN* Methylation Patterns

Among the 106 patients with longitudinally profiled IDH-wildtype glioblastoma, 12 patients (11%) developed somatic hypermutation at recurrence following temozolomide treatment consisting of a predominance of C>T:G>A transitions, which is the mutational signature known to arise in recurrent gliomas and other cancers due to the alkylating effects of temozolomide on the tumor genome.[3,37,38] This included 7 patients who developed this temozolomide-induced somatic hypermutation at the first surgically treated recurrence and 5 additional patients at the second surgically treated recurrence (Supplementary Figure S7 and Tables S3 and S5). Patients who developed somatic hypermutation posttemozolomide had a significantly longer interval from initial surgery until tumor recurrence than those who did not (27.8 vs. 10.4 months, $P < .001$) (Figure 5A, Supplementary Figure S8). In contrast to IDH-mutant gliomas where temozolomide-induced hypermutation is associated with poor prognosis,[39,41–43] those patients with IDH-wildtype glioblastoma who developed hypermutation posttemozolomide had significantly longer overall survival from initial surgery (67.9 vs. 20.7 months, $P < .001$) and also from the time of recurrence after the development of hypermutation (30.9 vs. 9.5 months, $P = .001$) compared with those patients who did not. There was no difference in oncogenic alteration frequency in initial treatment-naïve glioblastoma specimens that subsequently developed temozolomide-induced hypermutation versus those that did not (Supplementary Table S21). However, we identified 4 specific CpG sites out of 12 total interrogated sites in the promoter region of *MGMT* (which encodes a DNA repair enzyme), as well as multiple CpG sites in the promoter regions of *CCDC147*, *GCA*, and *KCNQ1DN* (which encodes a negative regulator of c-Myc),[44] that were significantly more methylated in those initial treatment-naïve glioblastoma which subsequently developed temozolomide-induced hypermutation compared with those that did not (Figure 5B, D, Supplementary Tables S27–S30). We then generated a composite score (ranging from 0 to 4) across the 4 critical CpG sites in the *MGMT* promoter based on the DNA methylation β-values in initial treatment-naïve tumors which could potentially be used prospectively to identify IDH-wildtype glioblastomas most likely to develop

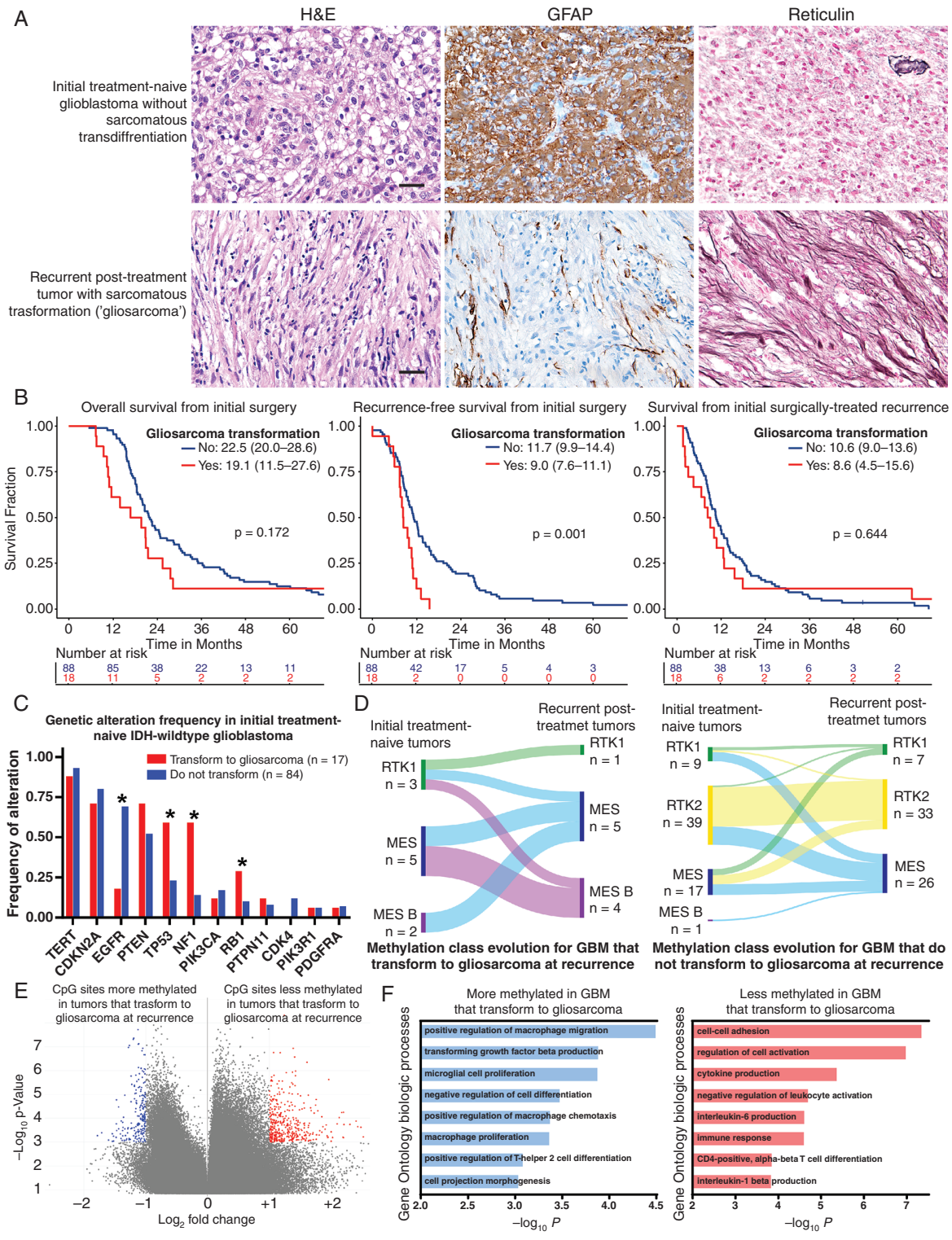


Figure 4. Sarcomatous transformation of IDH-wildtype glioblastoma at recurrence is determined by a unique cell state with a distinct molecular signature at initial resection before therapy. (A) Histopathology images of an initial treatment-naïve glioblastoma (top panels) show tumor cells with fibrillary glial processes, diffuse GFAP expression, and absence of intercellular reticulin meshwork. At the time of recurrence following adjuvant radiation and temozolomide chemotherapy, this glioblastoma developed MES transdifferentiation (bottom panels) with spindled tumor cells arranged in fascicles, loss of GFAP expression, and intercellular reticulin deposition. Scale bar = 100 μm. (B) Kaplan–Meier plots of overall survival from initial surgery (left), recurrence-free survival from initial surgery (middle), and survival from first surgically treated recurrence (right) for 106 patients with IDH-wildtype glioblastoma stratified by sarcomatous transformation at recurrence or not. Median estimated survival and 95% CIs are shown, as well as exact *P*-values by log-rank test. (C) Bar plot of genetic alteration frequency for the 12 most commonly altered oncogenes and tumor suppressor genes in 101 initial treatment-naïve IDH-wildtype glioblastomas stratified by sarcomatous transformation at recurrence or

not. Asterisks denote significant ($P < .05$) differences in genetic alteration frequency, specifically decreased *EGFR* and increased *TP53*, *NF1*, and *RB1* alterations in those tumors that transformed to gliosarcoma at recurrence. (D) Sankey plots of DNA methylation class assignment for matched initial treatment-naïve and first surgically treated recurrent IDH-wildtype glioblastomas using the DKFZ Molecular Neuropathology classifier tool version 12.5, stratified by the 10 tumors that transformed to gliosarcoma at recurrence (left) and the 66 tumors that did not transform to gliosarcoma. This analysis revealed enrichment for the MES methylation class and an absence of the RTK2 methylation class among those glioblastomas that underwent sarcomatous transformation. Additionally, there was enrichment for the novel MES B methylation subclass in those recurrent glioblastomas with sarcomatous transformation which was absent in those recurrent glioblastomas without sarcomatous transformation. (E) Volcano plot of genome-wide DNA methylation data from initial treatment-naïve glioblastoma tumor specimens that later transformed to gliosarcoma at the time of recurrence ($n = 17$) versus those that did not ($n = 81$). Each dot represents an individual CpG site in the genome that DNA methylation levels were interrogated at across the 98 initial treatment-naïve IDH-wildtype glioblastoma tumor samples. Blue dots on the left side of the plot represent those CpG sites which are significantly ($P < .001$) more methylated in those glioblastomas that transformed to gliosarcoma versus those that did not. Red dots on the right side of the plot represent those CpG sites which are significantly less methylated in those glioblastomas that transformed to gliosarcoma versus those that did not. (F) Gene Ontology biological processes that are significantly enriched ($P < .001$) in genes containing the most differentially methylated CpG sites in their upstream regulatory regions in those glioblastomas that transformed to gliosarcoma versus those that did not.

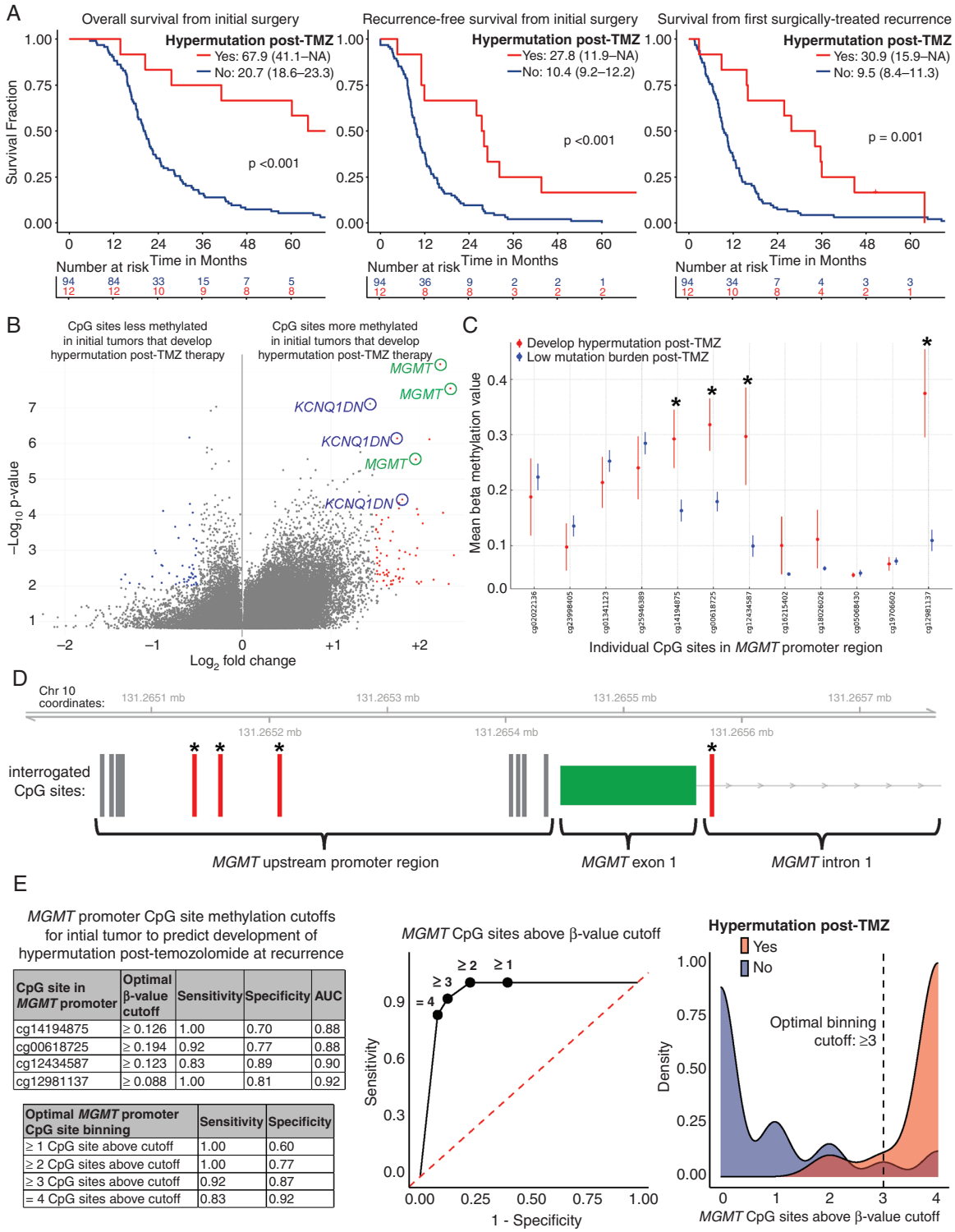
temozolomide-induced hypermutation associated with favorable survival. Based on the calculated β-value cutoff at each of these 4 sites, we determined that having 3 or more of the *MGMT* promoter methylation sites above the cutoff demonstrated a sensitivity of 92% and a specificity of 87% for identifying patients in this cohort that would go on to develop temozolomide-induced hypermutation at recurrence (Figure 5E).

Glioblastoma Survival-Associated DNA Methylation Evolution Signature

Given the heterogeneous epigenomic evolution patterns observed among IDH-wildtype glioblastomas, we sought to identify any CpG sites and associated genes/pathways whose differential methylation correlates with patient outcomes. We first generated a Δβ value matrix for each initial and recurrent tumor pair for 98 patients with IDH-wildtype glioblastoma, consisting of the change in DNA methylation β-value from initial to recurrent tumor specimens at each of the ~850,000 interrogated CpG sites. We then identified 347 specific CpG sites whose change in DNA methylation levels most significantly correlated with overall survival among the patient cohort. We then defined 3 patient subgroups based on mean Δβ value across the 347 CpG sites: Group A (mean $\Delta\beta > 0.0305$) was composed of those patients whose recurrent tumors became more methylated at the 347 CpG sites; Group B ($-0.0145 <$ mean $\Delta\beta \leq 0.0305$) was composed of those patients who had relatively stable methylation levels at recurrence; and Group C (mean $\Delta\beta \leq -0.0145$) was composed of those patients whose recurrent tumors became less methylated at the 347 CpG sites (Figure 6A, Supplementary Tables S31 and S32). This patient subgrouping by DNA methylation evolution signature correlated with overall survival ($P < .001$) and recurrence-free survival from initial surgery ($P < .001$), with patients in Group A demonstrating the most favorable clinical outcomes (median survival of 34.9 months) and patients in Group C demonstrating the least favorable outcomes (median survival of 16.3 months) (Figure 6B). While there were no significant differences in sex, age, tumor location, or adjuvant therapy amongst the 3 patient subgroups (Supplementary Table S1), there was an enrichment for *TP53* and *RB1* mutations in the tumors of Group C patients compared with the other 2 groups (Supplementary Table S21), as well as larger recurrent tumor volumes (both enhancing and nonenhancing) in the Group C patients (Supplementary Table S1). Multivariate analysis demonstrated that the 347 CpG site epigenomic evolution groups were independently correlated with overall and recurrence-free survival ($P < .05$; Supplementary Figure S9). Stratifying 42 patients with IDH-wildtype glioblastoma from an external cohort into 3 groups using this epigenomic evolution signature with the identical Δβ-value cutoffs revealed a similar pattern of overall survival and recurrence-free survival (Supplementary Figure S10 and Tables S33–S34).[17] Gene Ontology biological processes enriched in genes containing the 347 CpG sites revealed adrenergic receptor signaling and cyclic AMP signaling pathways as among the most significantly enriched whose differential methylation correlates with this survival-associated epigenomic evolution signature (Figure 6C, Supplementary Table S35).

Discussion

Similar to other recent longitudinal profiling studies,[3–21] our analyses demonstrate that glioblastoma is not a molecularly static disease but rather evolves both genetically and epigenetically during treatment and disease recurrence. While there is no predominant genetic event newly acquired or enriched in recurrent glioblastomas, analysis of paired initial and recurrent tumors identified that *TERT* promoter mutation and *CDKN2A* homozygous deletion are uniformly early events during gliomagenesis, whereas alterations involving other major oncogenes and tumor suppressor genes (eg *EGFR*, *PDGFRA*, *NF1*, *PIK3CA*, *PIK3R1*, *PTEN*, and *PTPN11*) occur later during gliomagenesis and are often subclonal or private to initial or recurrent tumor specimens. This important finding places renewed emphasis on efforts to therapeutically target tumor cell immortalization driven by *TERT* promoter mutation and cell cycle deregulation driven by *CDKN2A* inactivation as these represent the earliest key fundamental driving events in the majority of glioblastomas. Furthermore, this finding also may help to explain the challenge and past failures of therapeutically targeting EGFR and the PI3-kinase-Akt-MTOR pathway in glioblastoma given the later occurrence



CpG site in *MGMT* promoter	Optimal β-value cutoff	Sensitivity	Specificity	AUC
cg14194875	≥ 0.126	1.00	0.70	0.88
cg00618725	≥ 0.194	0.92	0.77	0.88
cg12434587	≥ 0.123	0.83	0.89	0.90
cg12981137	≥ 0.088	1.00	0.81	0.92

Optimal *MGMT* promoter CpG site binning	Sensitivity	Specificity
≥ 1 CpG site above cutoff	1.00	0.60
≥ 2 CpG sites above cutoff	1.00	0.77
≥ 3 CpG sites above cutoff	0.92	0.87
= 4 CpG sites above cutoff	0.83	0.92

Figure 5. Development of somatic hypermutation in response to alkylating chemotherapy with temozolomide for IDH-wildtype glioblastoma is dictated by DNA methylation at specific CpG sites in the promoter regions of *MGMT* and *KCNQ1DN*. (A) Kaplan–Meier plots of overall survival from initial surgery (left), recurrence-free survival from initial surgery (middle), and survival from first surgically treated recurrence (right) for 106 patients with IDH-wildtype glioblastoma stratified by the development of somatic hypermutation at recurrence following temozolomide treatment. Median estimated survival and 95% CIs are shown, as well as exact *P*-values by log-rank test. (B) Volcano plot of genome-wide DNA methylation data from initial treatment-naïve glioblastoma tumor specimens that became hypermutated at the time of recurrence following TMZ treatment ($n = 12$) versus those that did not ($n = 87$). Each dot represents an individual CpG site in the genome that DNA methylation levels were interrogated at across 99 initial treatment-naïve IDH-wildtype glioblastoma tumor samples. Red dots on the right side of the plot represent those CpG sites which are significantly ($P < .01$) more methylated in those glioblastomas that became hypermutated at recurrence following treatment

with temozolomide versus those that did not, which include multiple CpG sites in the upstream promoter region of the *MGMT* and *KCNQ1DN* genes. Blue dots on the left side of the plot represent those CpG sites which are significantly less methylated in those glioblastomas that became hypermutated at recurrence following treatment with temozolomide versus those that did not. (C) Scatter plot of mean DNA methylation values at the 12 interrogated CpG sites in the upstream regulatory region of *MGMT* in 99 initial treatment-naïve IDH-wildtype glioblastomas stratified by those that became hypermutated at recurrence following treatment with temozolomide versus those that did not. Asterisks mark the 4 CpG sites with significant differences in the mean DNA methylation β-values between the two subgroups. (D) Diagram of the upstream promoter region of *MGMT* showing the 12 interrogated CpG sites. Asterisks mark the 4 critical CpG sites (red bars) within the *MGMT* promoter whose differential methylation in initial treatment-naïve glioblastomas dictates whether they will go on to become hypermutated at the time of recurrence following TMZ treatment. No significant differences in DNA methylation levels were found at the other 8 CpG sites (gray bars). (E) Analysis determining the optimal DNA methylation β-value cutoffs for each of the 4 critical CpG sites in the *MGMT* promoter region and the optimal binning for a quantity of these 4 CpG sites above the cutoff for predicting whether an initial treatment-naïve IDH-wildtype glioblastoma is likely to develop somatic hypermutation at recurrence following treatment with temozolomide. Abbreviation: AUC = area under the curve.

of these genetic alterations and their subclonality in many patients.

Through longitudinal analysis of IDH-wildtype glioblastomas, we identified 3 distinct patterns of genomic alteration evolution that we termed stable, additive, and divergent. While subgrouping patients by the different genomic alteration evolution patterns did not correlate with survival in the setting of current standard-of-care therapy, assessing these patterns is critical for informing the best targeted therapy regimen at the time of recurrence. For example, patients in our cohort had switching of the activated receptor tyrosine kinase gene (eg *EGFR* amplified in initial specimen vs. *MET* amplified in recurrent specimen), as well as variant switching on the amplified *EGFR* alleles (eg *EGFRvIII* intragenic deletion in initial specimen vs. extracellular domain missense mutation in recurrent specimen), both of which have important ramifications for selecting appropriate targeted therapy agents.

We found that IDH-wildtype glioblastomas demonstrate heterogeneous epigenomic evolution patterns distinct from IDH-mutant astrocytomas. Whereas recurrent posttreatment IDH-mutant astrocytomas uniformly become less methylated, IDH-wildtype glioblastomas undergo heterogenous epigenomic evolution, with some becoming more globally methylated, some becoming less globally methylated, and some remaining relatively stable. This global methylation shift was not correlated with outcomes in this patient cohort treated with the current standard-of-care; however, these changes in global epigenomic patterns may likely denote unique biologic subgroups of glioblastoma with differential response to specific targeted agents and may inform future therapeutic studies targeting the underlying differentially methylated gene programs.

While the global hyper- versus hypomethylation shift from initial to recurrent glioblastoma specimens did not correlate with outcomes in this patient cohort, we identified that the DNA methylation shift at 347 specific CpG sites from initial to recurrent tumor specimens was significantly associated with both overall survival and recurrence-free survival for patients with IDH-wildtype glioblastoma in both our cohort and an external validation cohort.[17] Patients whose tumors became more methylated at recurrence at these specific 347 CpG sites had superior outcomes compared with patients whose tumors became less methylated. We therefore speculate that the biological pathways controlled by these 347 CpG sites may be critical to glioblastoma progression and associated with resistance to therapy. Several of these CpG sites are located in genes including *PDE4B*, *PDE4D*, *RAPGEF2*, and *FFAR4* that regulate adrenergic receptor signaling and cyclic AMP signaling, raising the possibility that this might be a critical therapeutic node to investigate in future studies.

A cellular phenotypic response to therapy that has been observed microscopically in a substantial subset of recurrent IDH-wildtype glioblastomas is sarcomatous transformation to "gliosarcoma." Historically, such gliosarcomas are thought to represent a potentially more aggressive subtype of glioblastoma which can invade into the overlying dura and calvarium.[45] However, the underlying biological basis of gliosarcoma transformation has not been resolved to date. Here, we show that glioblastomas which transform to gliosarcoma have earlier recurrence compared with conventional glioblastoma and harbor a unique epigenetic signature and mutational profile at the time of initial surgery prior to therapy and before microscopic evidence of MES transdifferentiation. This includes enrichment for *NF1*, *TP53*, and *RB1* inactivation, paucity of *EGFR* amplification/mutation, and differential methylation of CpG sites regulating immune cell and TGF-β signaling, which together suggest potential unique therapeutic vulnerabilities for affected patients. Identification of this molecular signature in an initial resection of glioblastoma corresponding to high propensity for sarcomatous transformation and early recurrence may warrant more aggressive or alternative therapy for patients, which we aim to test in future prospective clinical trials.

A more recently recognized therapy-induced phenomenon in gliomas treated with the alkylating agent temozolomide is the development of somatic hypermutation characterized by a predominance of C>T:G>A transitions. This temozolomide-induced hypermutation was first identified in lower-grade IDH-mutant gliomas at the time of recurrence, which has been found to correspond with high-grade transformation, increased risk of dissemination via cerebrospinal fluid, and poor outcomes.[41,43] In contrast, we found that IDH-wildtype glioblastomas which developed temozolomide-induced hypermutation occurred in those patients with the longest intervals between initial resection and recurrence and were associated with favorable overall survival from initial surgery and also from the time of recurrence after the development of somatic hypermutation. Somatic hypermutation in glioblastomas can be due to primary mismatch repair deficiency (either germline or somatic in origin) or secondary to iatrogenic alkylating chemotherapy.[36,41] While other studies

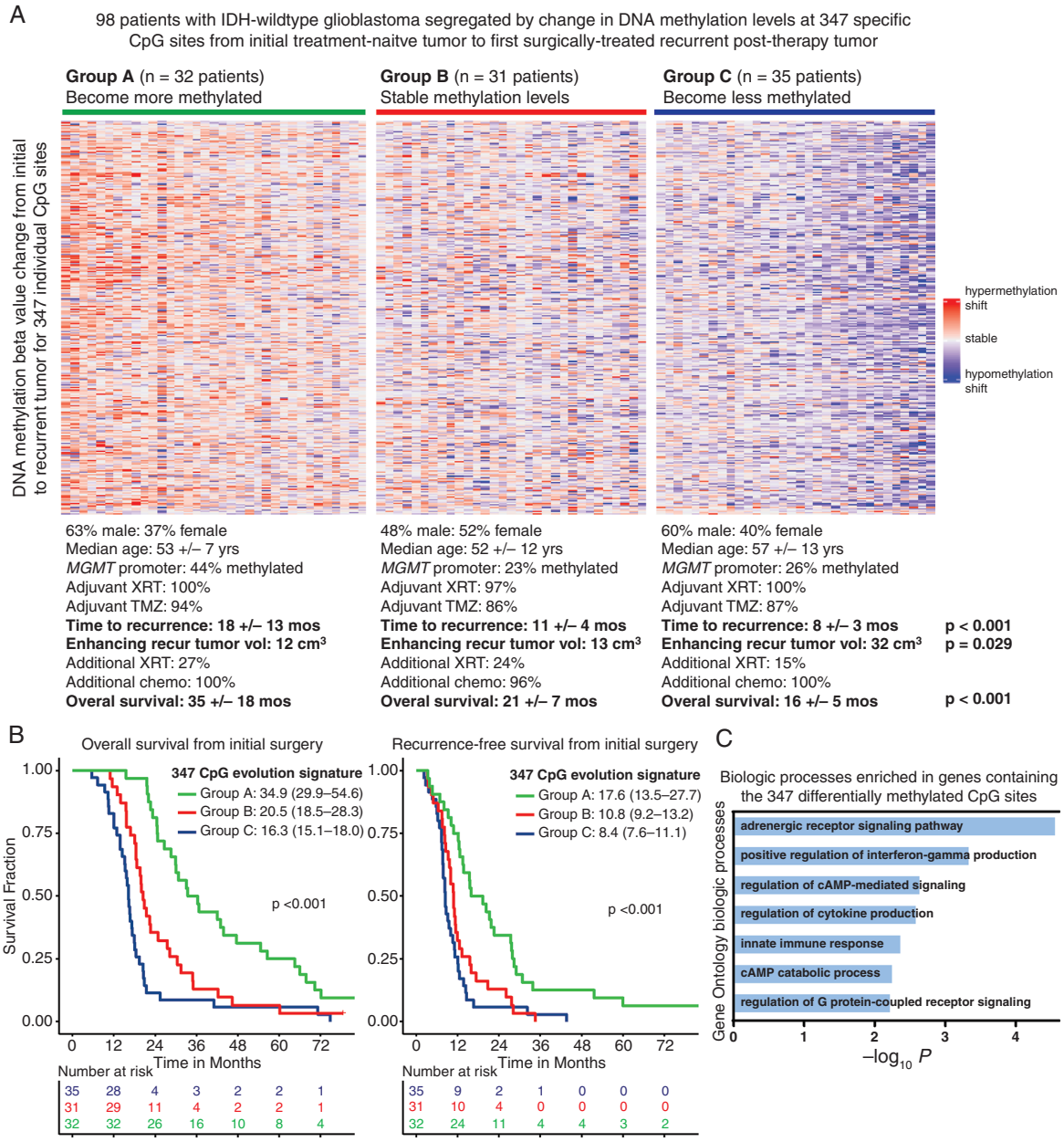


Figure 6. DNA methylation evolution at 347 specific CpG sites across the genome correlates with survival for patients with IDH-wildtype glioblastoma. (A) Heatmap of the DNA methylation β-value change (Δβ value) from initial treatment-naïve tumor to recurrent posttreatment tumor specimens at 347 CpG sites (rows) for a cohort of 98 patients (columns) with IDH-wildtype glioblastoma. The DNA methylation evolution at these 347 specific CpG sites segregated the patient cohort into 3 groups that significantly correlated with interval from initial resection to recurrence ($P < .001$), enhancing tumor volume at recurrence ($P = .029$), and overall survival ($P < .001$). Group A was composed of those patients whose tumors became more methylated at these 347 CpG sites from initial to recurrent tumors and was associated with superior survival, whereas Group C was composed of those patients whose tumors became less methylated at these 347 CpG sites from initial to recurrent tumors and was associated with inferior survival. (B) Kaplan–Meier plots of overall survival from initial surgery (left) and recurrence-free survival from initial surgery (right) for 98 patients with IDH-wildtype glioblastoma stratified by the 347 CpG site DNA methylation evolution subgroups. Median estimated survival and 95% CIs are shown, as well as exact *P*-values by log-rank test. (C) Gene Ontology biological processes that are significantly enriched ($P < .01$) in genes containing the 347 CpG sites composing the DNA methylation evolution signature for IDH-wildtype glioblastoma.

investigating clinical outcomes for hypermutated glioblastomas have not observed prolonged survival,[39] our patient population stratified exclusively by somatic hypermutation at recurrence following temozolomide therapy with Mutational Signature 11 experienced longer survival indicating a different biologic trajectory for these unique tumors. We did not observe any differences in the patient age, sex, tumor location, or genetic alteration profiles of those glioblastomas which developed this hypermutation posttemozolomide treatment. However, DNA methylation

profiling revealed that initial treatment-naïve glioblastomas with elevated methylation levels at 4 specific CpG sites in the *MGMT* promoter were significantly correlated with the development of temozolomide-induced hypermutation at recurrence compared with those with low methylation levels at these 4 *MGMT* CpG sites. Furthermore, we identified that elevated methylation levels at CpG sites in the *KCNQ1DN, CCDC147,* and *GCA* promoters also significantly correlated with subsequent development of hypermutation posttemozolomide treatment. These specific *MGMT* and other gene loci promoter methylation patterns could serve as biomarkers to identify those patients who will develop somatic hypermutation and experience favorable survival with temozolomide treatment, which requires validation in additional patient cohorts. Alternative therapeutic approaches leveraging this biologic vulnerability such as prolonged temozolomide treatment, potentially with accompanying immune checkpoint blockade, should be explored for this patient population.

Altogether, our analyses demonstrate that most glioblastomas undergo longitudinal genomic and epigenomic evolution in response to treatment with radiation and temozolomide, which likely underlie disease progression and the different patient trajectories observed clinically. We show that personalized genomic analysis of both initial treatment-naïve and recurrent posttreatment tumors can reveal genetic alterations underlying treatment resistance mechanisms (eg *EGFR* variant switching, temozolomide-induced hypermutation) that impact therapeutic decision making. Furthermore, prospective molecular profiling of the initial surgical specimen can identify biomarkers that predict which patients are most likely to follow certain progression trajectories including the development of sarcomatous transformation or somatic hypermutation associated with less favorable and more favorable outcomes, respectively. As such, we believe that precision medicine for glioblastoma requires the incorporation of genomic/epigenomic evolution analysis and needs to be predicated upon molecular studies performed on all available longitudinally obtained tumor specimens.

Supplementary Material

Supplementary material is available online at *Neuro-Oncology* (https://academic.oup.com/neuro-oncology).

Keywords

DNA methylation | glioblastoma | gliosarcoma | molecular neuropathology | temozolomide-induced hypermutation

Funding

This study was supported by the Panattoni Family Foundation and the UCSF Glioblastoma Precision Medicine Program sponsored by the Sandler Foundation. C.G.L. was supported by the UCSF Training Program in Translational Brain Tumor Research, National Cancer Institute, National Institutes of Health [T32 CA151022]. D.A.S. was also supported by the Morgan Adams Foundation, the Gilbert Family Foundation, the Yuvaan Tiwari Foundation, the Ross Family, the UCSF Department of Pathology Experimental Neuropathology Endowment Fund, the UCSF Program for Breakthrough Biomedical Research, and a Developmental Research Program Award from the UCSF Brain Tumor SPORE [P50 CA097257]. J.J.P. and the UCSF Brain Tumor Biorepository and Pathology Core were also supported by the UCSF Brain Tumor SPORE [P50 CA097257].

Acknowledgements

We thank the staff of the UCSF Clinical Cancer Genomics Laboratory and the UCSF Histology Laboratory for technical assistance, and Ken Probst for illustration support. We also thank our patients (the study participants) and the many providers and clinical staff at the UCSF Brain Tumor Center involved in the multidisciplinary care of these neuro-oncology patients.

Conflict of interest statement

Jennie Taylor, John de Groot, Annette Molinaro, Joseph Costello, Aaron Diaz, Susan Chang, and Mitchel Berger are members of the editorial board of *Neuro-Oncology* but were not involved in the handling or decision making for this manuscript. Jennie Taylor receives grant support from Bristol Myers Squibb and Servier Pharmaceuticals and serves on the advisory board for Servier Pharmaceuticals. The remaining authors declare that they have no competing interests related to this study.

Author contributions

All authors made substantial contributions to the conception or design of the study; the acquisition, analysis, or interpretation of data; or drafting and revising the manuscript. All authors approved the manuscript. All authors agree to be personally accountable for individual contributions and to ensure that questions related to the accuracy or integrity of any part of the work are appropriately investigated, resolved, and the resolution documented in the literature. S.M.C., M.S.B., and D.A.S. designed the study and analyses. Tissue banking and tumor specimen management were performed by A.S., J.J.P., and D.A.S. Tumor nucleic acid extraction and DNA methylation array data generation was performed by J.W., A.R., and D.A.S. Genomic analysis was performed by C.G.L. and D.A.S. Methylation data analysis was performed by C.G.L., N.A.A., R.G., and D.A.S. Clinical data extraction and statistical analysis were performed by C.G.L., N.A.A., J.S.Y., R.A.M., and D.A.S. Pathologic assessment was performed by C.G.L., M.P., A.P., A.W.B., and D.A.S. Radiologic assessment was performed by J.E.V.M. Neurosurgical patient management was performed by J.S.Y., R.A.M., P.V.T., M.K.A., E.F.C., S.L.H.J., and M.S.B. Radiation oncology patient management was performed by D.R.R. Neuro-oncologic patient management was performed by N.A.O.B.,

J.W.T., J.D.G., J.L.C., N.A.B., and S.M.C. The study was supervised by A.M.M., J.F.C., A.A.D., S.M.C., M.S.B., and D.A.S. The manuscript and figures were prepared by C.G.L., N.A.A., J.S.Y., R.G., and D.A.S. with input from all authors.

Ethical approval

This study was approved by the Committee on Human Research of the University of California, San Francisco, with a waiver of patient consent.

Data availability

Patient-level clinical and treatment data are provided in the supplementary tables. Raw and processed DNA methylation data from the longitudinal IDH-wildtype glioblastoma cohort and the longitudinal IDH-mutant astrocytoma cohort have been deposited at the NCBI Gene Expression Omnibus (GEO) under accession numbers GSE279073 and GSE260850, respectively. Annotated DNA sequencing data from the longitudinal IDH-wildtype glioblastoma cohort are provided in the supplementary tables. Raw sequencing data files are available from the authors upon request.

Affiliations

UCSF Brain Tumor Center, University of California, San Francisco, California, USA (C.-H.G.L., N.N.A.-A., J.S.Y., R.G., R.A.M., J.W., A.R., A.S., N.A.O.B., J.W.T., J.G., J.E.V.-M., M.P., A.P., A.W.B., P.V.T., M.K.A., E.F.C., S.L.H.-J., D.R.R., A.M.M., J.F.C., A.A.D., J.L.C., N.A.B., J.J.P., S.M.C., M.S.B., D.A.S.); Department of Pathology, University of California, San Francisco, California, USA (C.-H.G.L., R.G., J.W., A.R., M.P., A.P., A.W.B., D.R.R., J.J.P., D.A.S.); Department of Pathology, Johns Hopkins University, Baltimore, Maryland, USA (C.-H.G.L.); Department of Neurological Surgery, University of California, San Francisco, California, USA (N.N.A.-A., J.S.Y., R.A.M., A.S., A.P., P.V.T., M.K.A., E.F.C., S.L.H.-J., D.R.R., A.M.M., J.F.C., A.A.D., J.J.P., M.S.B.); Division of Neuro-Oncology, Department of Neurological Surgery, University of California, San Francisco, California, USA (N.A.O.B., J.W.T., J.G., J.L.C., N.A.B., S.M.C.); Department of Neurology, University of California, San Francisco, California, USA (N.A.O.B., J.W.T., J.G., J.L.C.); Department of Radiology & Biomedical Imaging, University of California, San Francisco, California, USA (J.E.V.-M.); Department of Radiation Oncology, University of California, San Francisco, California, USA (D.R.R.)

References

1. Stupp R, Mason WP, van den Bent MJ, et al. Radiotherapy plus concomitant and adjuvant temozolomide for glioblastoma. *N Engl J Med.* 2005; 352(10):987–996.
2. Young JS, Morshed RA, Hervey-Jumper SL, Berger MS. The surgical management of diffuse gliomas: current state of neurosurgical management and future directions. *Neuro-Oncology.* 2023; 25(12):2117–2133.
3. Johnson BE, Mazor T, Hong C, et al. Mutational analysis reveals the origin and therapy-driven evolution of recurrent glioma. *Science.* 2014; 343(6167):189–193.
4. van Thuijl HF, Mazor T, Johnson BE, et al. Evolution of DNA repair defects during malignant progression of low-grade gliomas after temozolomide treatment. *Acta Neuropathol.* 2015; 129(4):597–607.
5. Kim H, Zheng S, Amini SS, et al. Whole-genome and multisector exome sequencing of primary and post-treatment glioblastoma reveals patterns of tumor evolution. *Genome Res.* 2015; 25(3):316–327.
6. Kim J, Lee IH, Cho HJ, et al. Spatiotemporal evolution of the primary glioblastoma genome. *Cancer Cell.* 2015; 28(3):318–328.
7. Ceccarelli M, Barthel FP, Malta TM, et al. Molecular profiling reveals biologically discrete subsets and pathways of progression in diffuse glioma. *Cell.* 2016; 164(3):550–563.
8. Wang J, Cazzato E, Ladewig E, et al. Clonal evolution of glioblastoma under therapy. *Nat Genet.* 2016; 48(7):768–776.
9. Lee JK, Wang J, Sa JK, et al. Spatiotemporal genomic architecture informs precision oncology in glioblastoma. *Nat Genet.* 2017; 49(4):594–599.
10. GLASS C. Glioma through the looking GLASS: molecular evolution of diffuse gliomas and the Glioma Longitudinal Analysis Consortium. *Neuro Oncol.* 2018; 20(7):873–884.
11. Barthel FP, Wesseling P, Verhaak RGW. Reconstructing the molecular life history of gliomas. *Acta Neuropathol.* 2018; 135(5):649–670.
12. Barthel FP, Johnson KC, GLASS Consortium, et al. Longitudinal molecular trajectories of diffuse glioma in adults. *Nature.* 2019; 576(7785):112–120.
13. Draaisma K, Chatzipli A, Taphoorn M, et al. Molecular evolution of IDH wild-type glioblastomas treated with standard of care affects survival and design of precision medicine trials: a report from the EORTC 1542 study. *J Clin Oncol.* 2020; 38(1):81–99.
14. Neftel C, Laffy J, Filbin MG, et al. An integrative model of cellular states, plasticity, and genetics for glioblastoma. *Cell.* 2019; 178(4):835–849.e21.
15. Tanner G, Barrow R, Ajaib S, et al. IDHwt glioblastomas can be stratified by their transcriptional response to standard treatment, with implications for targeted therapy. *Genome Biol.* 2024; 25(1):45.
16. Drexler R, Khatri R, Schüller U, et al. Temporal change of DNA methylation subclasses between matched newly diagnosed and recurrent glioblastoma. *Acta Neuropathol.* 2024; 147(1):21.
17. Malta TM, Sabedot TS, Consortium The GLASS, et al. The epigenetic evolution of glioma is determined by the IDH1 mutation status and treatment regimen. *Cancer Res.* 2024; 84(5):741–756.
18. Wang L, Jung J, Babikir H, et al. A single-cell atlas of glioblastoma evolution under therapy reveals cell-intrinsic and cell-extrinsic therapeutic targets. *Nat Cancer.* 2022; 3(12):1534–1552.
19. Chaligne R, Gaiti F, Silverbush D, et al. Epigenetic encoding, heritability and plasticity of glioma transcriptional cell states. *Nat Genet.* 2021; 53(10):1469–1479.
20. Wang Q, Hu B, Hu X, et al. Tumor evolution of glioma-intrinsic gene expression subtypes associates with immunological changes in the microenvironment. *Cancer Cell.* 2017; 33(1):152–156.
21. Varn FS, Johnson KC, GLASS Consortium, et al. Glioma progression is shaped by genetic evolution and microenvironment interactions. *Cell.* 2022; 185(12):2184–2199.e16.
22. Verhaak RG, Hoadley KA, Purdom E, et al. Integrated genomic analysis identifies clinically relevant subtypes of glioblastoma characterized by abnormalities in PDGFRA, IDH1, EGFR, and NF1. *Cancer Cell.* 2010; 17(1):98–110.
23. Brennan CW, Verhaak RG, TCGA Research Network, et al. The somatic genomic landscape of glioblastoma. *Cell.* 2013; 155(2):462–477.
24. Capper D, Jones DTW, Sill M, et al. DNA methylation-based classification of central nervous system tumours. *Nature.* 2018; 555(7697):469–474.

25. Wu Y, Fletcher M, Gu Z, et al. Glioblastoma epigenome profiling identifies SOX10 as a master regulator of molecular tumour subtype. *Nat Commun*. 2020; 11(1):6434.
26. Verburg N, Barthel FP, Anderson KJ, et al. Spatial concordance of DNA methylation classification in diffuse glioma. *Neuro-Oncology*. 2021;23(12):2054–2065.
27. Singh O, Pratt D, Aldape K. Immune cell deconvolution of bulk DNA methylation data reveals an association with methylation class, key somatic alterations, and cell state in glial/glioneuronal tumors. *Acta Neuropathol Commun*. 2021; 9(1):148.
28. Drexler R, Khatri R, Sauvigny T, et al. A prognostic neural epigenetic signature in high-grade glioma. *Nat Med*. 2024; 30(6):1622–1635.
29. Eckhardt A, Drexler R, Schoof M, et al. Mean global DNA methylation serves as independent prognostic marker in IDH-wildtype glioblastoma. *Neuro Oncol*. 2024; 26(3):503–513.
30. Karschnia P, Vogelbaum MA, van den Bent M, et al. Evidence-based recommendations on categories for extent of resection in diffuse glioma. *Eur J Cancer*. 2021; 149:23–33.
31. Karschnia P, Young JS, Dono A, et al. Prognostic validation of a new classification system for extent of resection in glioblastoma: a report of the RANO resect group. *Neuro Oncol*. 2023; 25(5):940–954.
32. Kline CN, Joseph NM, Grenert JP, et al. Targeted next-generation sequencing of pediatric neuro-oncology patients improves diagnosis, identifies pathogenic germline mutations, and directs targeted therapy. *Neuro Oncol*. 2017; 19(5):699–709.
33. Zhang Y, Lucas CG, Young JS, et al. Prospective genomically guided identification of "early/evolving" and "undersampled" IDH-wildtype glioblastoma leads to improved clinical outcomes. *Neuro Oncol*. 2022; 24(10):1749–1762.
34. Lucas CG, Sloan EA, Gupta R, et al. Multiplatform molecular analyses refine classification of gliomas arising in patients with neurofibromatosis type 1. *Acta Neuropathol*. 2022; 144(4):747–765.
35. Williams EA, Ravindranathan A, Gupta R, et al. Novel SOX10 indel mutations drive schwannomas through impaired transactivation of myelination gene programs. *Neuro Oncol*. 2023; 25(12):2221–2236.
36. Hadad S, Gupta R, Oberheim Bush NA, et al. "De novo replication repair deficient glioblastoma, IDH-wildtype" is a distinct glioblastoma subtype in adults that may benefit from immune checkpoint blockade. *Acta Neuropathol*. 2023; 147(1):3.
37. Alexandrov LB, Nik-Zainal S, Wedge DC, et al; Australian Pancreatic Cancer Genome Initiative. Signatures of mutational processes in human cancer. *Nature*. 2013; 500(7463):415–421.
38. Campbell BB, Light N, Fabrizio D, et al. Comprehensive analysis of hypermutation in human cancer. *Cell*. 2017; 171(5):1042–1056.e10.e10.
39. Touat M, Li YY, Boynton AN, et al. Mechanisms and therapeutic implications of hypermutation in gliomas. *Nature*. 2020; 580(7804):517–523.
40. Capper D, Stichel D, Sahm F, et al. Practical implementation of DNA methylation and copy-number-based CNS tumor diagnostics: the Heidelberg experience. *Acta Neuropathol*. 2018; 136(2):181–210.
41. Choi S, Yu Y, Grimmer MR, et al. Temozolomide-associated hypermutation in gliomas. *Neuro Oncol*. 2018;20(10):1300–1309.
42. Mathur R, Zhang Y, Grimmer MR, et al. MGMT promoter methylation level in newly diagnosed low-grade glioma is a predictor of hypermutation at recurrence. *Neuro Oncol*. 2020; 22(11):1580–1590.
43. Yu Y, Villanueva-Meyer J, Grimmer MR, et al. Temozolomide-induced hypermutation is associated with distant recurrence and reduced survival after high-grade transformation of low-grade IDH-mutant gliomas. *Neuro Oncol*. 2021; 23(11):1872–1884.
44. Yang F, Wu Q, Zhang L, et al. The long noncoding RNA KCNQ1DN suppresses the survival of renal cell carcinoma cells through downregulating c-Myc. *J Cancer*. 2019; 10(19):4662–4670.
45. Galanis E, Buckner JC, Dinapoli RP, et al. Clinical outcome of gliosarcoma compared with glioblastoma multiforme: North Central Cancer Treatment Group results. *J Neurosurg*. 1998; 89(3):425–430.